New Journal of Physics
An Institute of Physics and Deutsche Physikalische Gesellschaft Journal

Measuring the interaction law of dissipative solitons

H U Bödeker[1,3], A W Liehr[1], T D Frank[2], R Friedrich[2] and H-G Purwins[1]

[1] Institut für Angewandte Physik, Corrensstr. 2/4, D-48149 Münster, Germany
[2] Institut für Theoretische Physik, Wilhelm-Klemm-Str. 9, D-48149 Münster, Germany
E-mail: boedeker@uni-muenster.de

New Journal of Physics **6** (2004) 62
Received 12 February 2004
Published 14 June 2004
Online at http://www.njp.org/
doi:10.1088/1367-2630/6/1/062

Abstract. We investigate the interaction of self-organized solitary current filaments (dissipative solitons) under the influence of noise in a planar dc gas-discharge system with high-ohmic barrier. These localized structures exhibit interesting properties such as propagation and scattering as well as the transient formation of molecules and clusters. To quantitatively examine these interesting properties, methods of stochastic data analysis are developed to determine interaction laws from experimentally recorded data series. It turns out that in most cases, the sign of the resulting interaction functions alternates with the distance of the dissipative solitons. This phenomenon can be connected to experimentally detectable oscillatorily decaying tails of the filaments, which is in agreement with theoretical predictions.

[3] Author to whom any correspondence should be addressed.

PII: S1367-2630(04)76006-1

Contents

1. Introduction

A central concern of modern science is to explain the mechanisms of complex processes of pattern formation which can be observed in nature in various fields. Mostly, complex structures consist of smaller substructures, which may have a complex substructure of their own. Typical examples for such systems can be found in biology, where life forms are made up of different organs which are composed of cells, again having a complex build-up. Usually, an insight has to be gained on the basis of simple systems before a transfer to more complex systems like extended biological structures can be made. Taking this into regard, we investigate the dynamics of elementary solitary structures in dissipative systems, which we refer to as *dissipative solitons* (DSs), following [1, 2]. These particle-like structures can be observed in various different systems, e.g. in biological systems as nerve pulses [3], in chemical systems as concentration drops of chemical reagents [4]–[6] or in optical systems as bright spots in the transversal plane of propagating laser beams [7, 8].

The formation of stable bound states of several DSs in dissipative systems is predicted by different types of model equations [9]–[11]. These predictions can be compared with observations in experimental systems, where localized dissipative structures may form stable stationary molecules and clusters [12]–[14]. However, as localized structures often possess neutral modes of translation which make them susceptible to various sorts of fluctuations, many experimental systems exist in which the interaction between the individual structures manifests itself only in transient processes [15, 16].

An important class of systems in which interaction of DS under the influence of fluctuations can be observed is dc gas-discharge systems with high ohmic semiconductor barrier. In these systems, the DSs appear in the form of localized current filaments. Their dynamics is strongly noise-influenced and therefore needs to be described by stochastic evolution equations such as Langevin equations. This opens the possibility to apply data-driven stochastic time-series analysis techniques [17] to extract deterministic and stochastic parts from experimentally recorded trajectories of single filaments [18, 19]. Overcoming the restriction to single filaments,

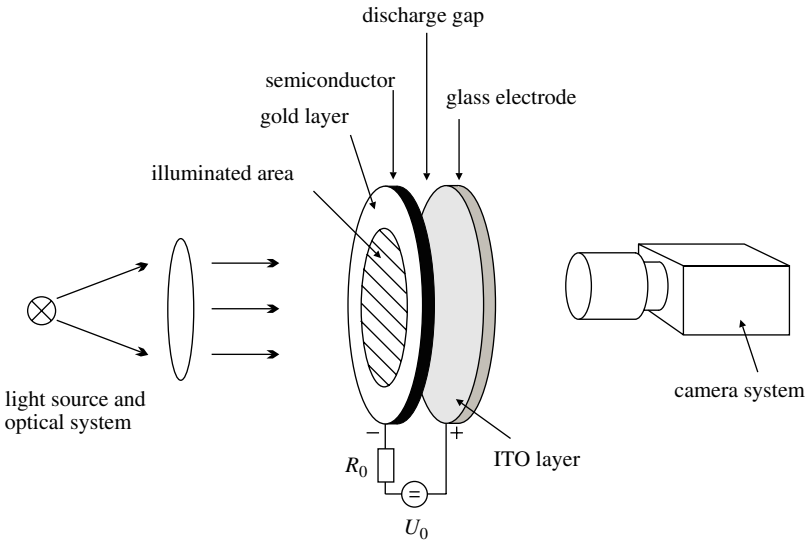

Figure 1. Schematic of the experimental dc gas-discharge system consisting of a high ohmic semiconductor electrode, a discharge gap filled with nitrogen and a transparent ITO electrode.

we present a stochastic data analysis method which is suitable for the measurement of the interaction law between the filaments. Using this approach, it is possible for the first time not only to experimentally analyse stationary states, but also to analyse the dynamics of transient states, enabling various applications in different branches of physics, which makes the presented technique a topic of broad interest. In the case of the investigated dc gas-discharge system the results of the analysis can be related to predictions of a system of model equations developed for the experimental system by interpreting it in the context of reaction–diffusion systems.

The paper is organized as follows: section 2 describes the experimental system and the applied recording techniques as well as the typical interaction processes that can be observed in the experiment. Section 3 recalls how stochastic data analysis techniques can be used for the investigation of the dynamics of isolated DSs and how an extension of these techniques to determine the interaction law between several DSs can be made. The results of the application of the new technique to experimental data are given in section 4. To have an understanding of the experimental findings, one may consider a phenomenological three-component reaction–diffusion system (section 5). The paper closes with a summary and an outlook in section 6.

2. The experiment

2.1. Experimental set-up

The investigated dc gas-discharge system (figure 1) consists of a high-ohmic semiconductor electrode (chromium-doped GaAs cooled to $T = 100\,\mathrm{K}$) contacted from one side with a semitransparent gold layer as anode, a gas gap with discharge length $d = 0.5\,\mathrm{mm}$ filled with

nitrogen of purity 99.999%, and a cathode made of glass and coated with a layer of indium tin oxide (ITO) being transparent for visible light. The semiconductor electrode exhibits a linear current–voltage characteristic. The specific resistivity of the semiconductor material takes values of $\rho_{SC} \approx 10^5$–$10^9\ \Omega\,\mathrm{cm}$ and can be controlled via the internal photo effect using an external light source. The discharge is driven by a constant voltage U_0 of several kV, whereas the global current is limited due to a large series resistor R_0 of some MΩ.

In the investigated current density range, the luminance radiation density emitted from the discharge gap in the visible spectrum is proportional to the average current density in the discharge direction [20]. Consequently, the dynamical behaviour of the gas discharge and in particular of self-organized current patterns in the discharge gap can be recorded through the ITO layer by ordinary camera techniques operating in the visible. Thereby, the originally three-dimensional patterns are observed as two-dimensional objects in the discharge plane, which is justified as they are quasi-two-dimensional due to the aspect ratio of the discharge space. In the presented case, a CCD camera with video frequency has been used to observe the patterns in the discharge gap.

For the following investigations, the parameters of the system were chosen in such a way that single or multiple DSs could be observed in the discharge. To analyse the dynamics of the filaments, their trajectories are extracted from the recorded images, identifying each filament as a connected region of high luminance density and then generating the trajectories of their centre of luminance using a nearest-neighbour tracing algorithm.

During the preparation of the experimental set-up, great care is taken to assure the spatial homogeneity of the system. An examination of the homogeneity can take place by igniting a homogeneous discharge over the whole discharge area or by analysing statistical properties of propagating DSs (see [18] for details).

2.2. Experimentally observable interaction processes

By analysing the dynamics of isolated filaments, it turns out that the DSs propagate under the influence of noise [18, 19], which might be related to noise in the semiconductor (generation-recombination, $1/f$ noise), thermal fluctuations in the gas and noisy processes of charge transportation through the semiconductor–gas discharge interface [21]. Naturally, the same holds for the interaction of several DSs. In spite of this, one can conclude from the direct observation of the trajectories of the DSs that they interact in a characteristic way.

In the following two different cases are presented. For certain choices of parameters, the DSs move rather slowly and the influence of fluctuations is only weak. In this case, a transient formation of soliton molecules can take place (figure 2). In the presented example, two DSs form a bound state over $t \approx 37$ s. Although the molecule rotates and both DSs show an irregular motion on a short time scale, the evolution of the distance of the DSs shows that the deviation from the average binding distance is rather small. Finally, the molecule breaks up and the DSs propagate independently. If the parameters are chosen differently, another typical interaction process can be observed: the scattering of the solitons. For such processes, the speed of the DSs is higher than in the first example and the fluctuations are usually much stronger. A typical example is depicted in figure 3. One can see from the figure that the DSs approach each other until they reach a minimal distance; afterwards the distance increases again. When observing many scattering processes, it turns out that the minimal distances are not arbitrary, but are always within a characteristic interval.

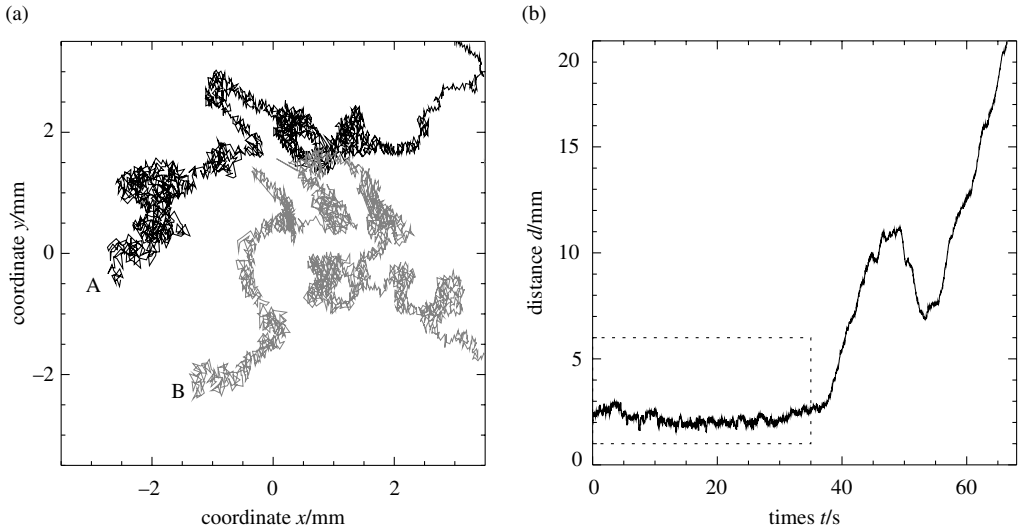

Figure 2. (a) Typical experimental trajectories generated by two current filaments recorded in the system presented in figure 1. The letters A and B denote the starting points of the filaments. (b) Time-dependant distance of the filaments, indicating the formation of a bound state (see (a)) followed by a separation of the filaments. Parameters: global voltage $U_0 = 3100\,\mathrm{V}$, specific resistivity of the semiconductor $\rho_{SC} = 4.19\,\mathrm{M\Omega\,cm}$, series resistor $R_0 = 4.4\,\mathrm{M\Omega}$, pressure $p = 276\,\mathrm{hPa}$, temperature $T = 100\,\mathrm{K}$, discharge gap width $d = 450\,\mu\mathrm{m}$, exposure time $t_{exp} = 0.02\,\mathrm{s}$, observed global current $I = 170\,\mu\mathrm{A}$.

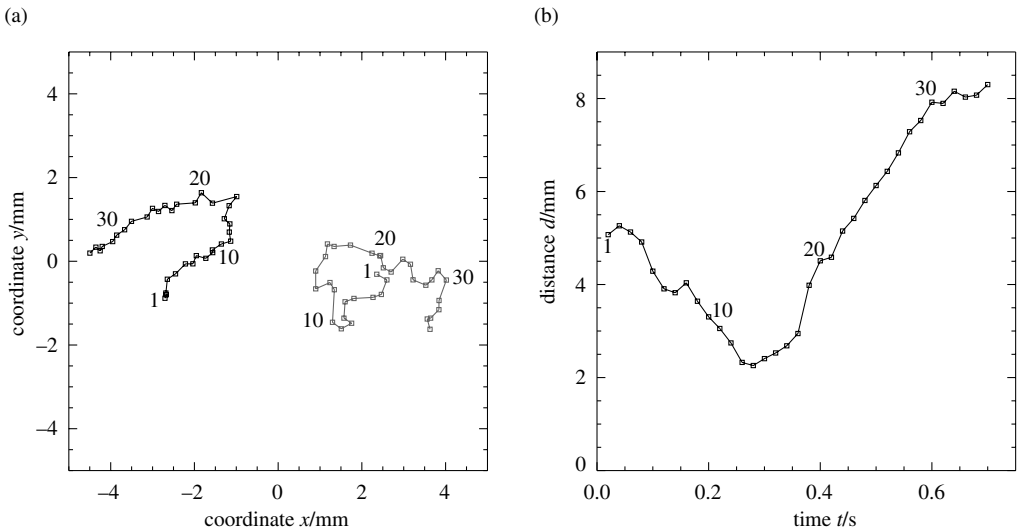

Figure 3. Typical scattering process for two DSs: trajectories (a) and temporal evolution of the soliton distance (b). Parameters: $U_0 = 3700\,\mathrm{V}$, $\rho_{SC} = 1.52 \times 10^6\,\Omega\,\mathrm{cm}$, $R_0 = 4.4\,\mathrm{M\Omega}$, $p = 271\,\mathrm{hPa}$, $T_{SC} = 100\,\mathrm{K}$, $d = 500\,\mu\mathrm{m}$ and $I = 300\,\mu\mathrm{A}$.

3. Stochastic data analysis

The observations described above allow for some basic conclusions of the nature of the interaction law between the DSs, but for strong fluctuations in particular, no precise quantitative statements can be made directly. As extensively discussed in [18], methods of stochastic data analysis can be used to separate deterministic and stochastic parts of the soliton dynamics for single DSs. It turns out that these methods can be generalized to quantitatively determine an interaction law between several DSs under the influence of noise. In this section, the fundamentals of stochastic data analysis for the dynamics of isolated DSs will be shortly recapitulated before discussing the extensions needed for the determination of the interaction law.

3.1. Analysis of isolated DSs

For the purpose of describing the motion of DSs in the quasi-two-dimensional gas-discharge plane, a particle approach is chosen, using the 'centre of luminance' $\boldsymbol{p}(t) = (p_x(t), p_y(t))^{\mathrm{T}}$ and the velocity $\dot{\boldsymbol{p}}(t) = \boldsymbol{v}(t) = (v_x(t), v_y(t))^{\mathrm{T}}$ of each individual filament as dynamic variables [19]. Motivated by theoretical considerations, the dynamics of the DSs is modelled by stochastic differential equations, i.e. Langevin equations.

As great care was taken to assure the spatially homogeneous preparation of the discharge system, one may assume O(2) symmetry (under negligence of the finite size of the system). Under these conditions, the following Langevin equation describing the dynamics of a single filament without interaction and external forces can be derived [19]:

$$\dot{\boldsymbol{v}}(t) = \boldsymbol{h}(\boldsymbol{v}(t)) + \underline{\boldsymbol{R}}(\boldsymbol{v}(t))\boldsymbol{\Gamma}(t). \tag{1}$$

In this equation, the acceleration of the DS is due to the co-action of a deterministic part $\boldsymbol{h}(\boldsymbol{v})$ resulting from inner degrees of freedom of the DS and a stochastic part $\underline{\boldsymbol{R}}(\boldsymbol{v})\boldsymbol{\Gamma}$, representing the influence of spatiotemporal fluctuations. The second expression is the product of a matrix of (velocity-dependent) noise amplitudes and a vector of Gaussian-distributed fluctuating noise forces, which are assumed to be δ-correlated on the time scale of the dynamics of the velocities:

$$\langle \Gamma_\mu(t) \rangle = 0, \qquad \mu = x, y, \tag{2}$$

$$\langle \Gamma_\mu(t)\Gamma_\nu(t') \rangle = 2\delta_{\mu\nu}\delta(t - t'), \qquad \mu, \nu = x, y. \tag{3}$$

Using the symmetry of the system, it is possible to simplify equation (1), yielding

$$\dot{\boldsymbol{v}} = h_v(v)\boldsymbol{e}_{\boldsymbol{v}} + R(v)\boldsymbol{\Gamma}(t) \tag{4}$$

with $\boldsymbol{e}_{\boldsymbol{v}} = \boldsymbol{v}/v$. With the validity of (1)–(3), the deterministic part of the acceleration can be determined from experimental data as

$$\boldsymbol{h}(\boldsymbol{v}) = \lim_{\Delta t \to 0} \frac{1}{\Delta t} \langle \tilde{\boldsymbol{v}}(t + \Delta t) - \tilde{\boldsymbol{v}}(t) \rangle |_{\tilde{\boldsymbol{v}}(t) = \boldsymbol{v}} \tag{5}$$

if $\tilde{\boldsymbol{v}}$ is a solution of (1). In a similar way, the amplitude of the fluctuations introduced in equation (4) can be estimated via

$$R^2(v) = \lim_{\Delta t \to 0} \frac{1}{2\Delta t} \langle (\tilde{v}(t + \Delta t) - \tilde{v}(t))^2 \rangle |_{\tilde{v}(t) = v}. \tag{6}$$

Note that the terms on the right-hand side of equations (5) and (6) actually yield the drift and diffusion coefficients of the Fokker–Planck equation corresponding to the Langevin equation (4). In the case of additive noise (i.e. $R(v) = \text{const.}$), the coefficients always correspond to the left-hand side of (5) and (6), respectively. In the case of multiplicative noise ($R(v) \neq \text{const.}$), the fluctuation term in (4) has to be interpreted according to Itó. If an interpretation according to Stratonovich or a generalized Stratonovich integral is used, spurious drift terms have to be added to the function $\boldsymbol{h}(\boldsymbol{v})$ in equation (5), which vanish for additive noise [22, 23]. Considering e.g. the Stratonovich case, the function $\boldsymbol{h}(\boldsymbol{v})$ must be replaced by a function $\hat{\boldsymbol{h}}(\boldsymbol{v})$ defined by

$$\hat{h}_\mu = h_\mu - R_{\nu\rho}\frac{\partial}{\partial v_\nu}R_{\mu\rho}, \quad \mu, \nu, \rho = x, y. \tag{7}$$

In addition, the noise term has to be interpreted according to Stratonovich. In any case, the conditional average on the right-hand side of equation (5) yields the total driving force that acts on the DSs being studied. This total driving force may or may not involve a noise-dependent contribution (i.e. a spurious drift).

In practice, one faces certain problems using (5) and (6) as

(i) the assumption (3) of δ-correlated noise will not be fulfilled (according to the Wiener–Kintchine theorem, this would mean a constant power spectrum),

(ii) the time between two data points will always be finite,

(iii) the amount of experimental data for the averaging process will be limited.

Therefore, one may replace the exact times $\Delta t \to 0$ by a small but finite time step. It is then possible to show that relations (5) and (6) stay approximately correct, i.e.

$$\boldsymbol{h}(\boldsymbol{v}) \approx \frac{1}{\Delta t}\langle(\tilde{\boldsymbol{v}}(t+\Delta t) - \tilde{\boldsymbol{v}}(t)\rangle|_{\tilde{\boldsymbol{v}}(t)\approx\boldsymbol{v}} \tag{8}$$

and

$$R^2(v) \approx \frac{1}{2\Delta t}\langle(\tilde{v}(t+\Delta t) - \tilde{v}(t))^2\rangle|_{\tilde{v}(t)\approx v}, \tag{9}$$

if the time step Δt is small compared with the characteristic time scale of the dynamics, but large enough compared with the time scale on which the noise-correlation decays. Relation (8) offers a possibility to determine the deterministic part of the Langevin equation from experimental data series, but unfortunately, even with the approximations made the number of available data points for the discussed experiment is so small that the result has a rather unsatisfying resolution. To overcome this problem, a method was developed in [18] to exploit the symmetry of equation (4) and estimate the radially symmetric function $h_v(v)$ via

$$h_v(v) \approx \frac{1}{\Delta t}\left\langle\frac{(\tilde{\boldsymbol{v}}(t+\Delta t) - \tilde{\boldsymbol{v}}(t))\cdot\tilde{\boldsymbol{v}}(t)}{\tilde{v}(t)}\right\rangle\Bigg|_{\tilde{\boldsymbol{v}}(t)\approx\boldsymbol{v}}. \tag{10}$$

In [18] the relation was proven for additive noise, as it was found using equation (9) that for the analysed experimental data series $R(v) = R = \text{const}$. However, it is worth noting that the relation also holds for multiplicative noise; for a proof, see appendix A1. Using equation (10), the accuracy of the result is strongly improved compared with (5).

Systematic experimental investigations [18] have shown that the experimentally determined drift term $h_v(v)$ can be represented by the polynomial

$$h_v(v) = a_1 v + a_3 v^3, \tag{11}$$

which, depending on the parameters a_1 and a_3, corresponds to overdamped and purely noise-driven DSs ($a_1 < 0, a_3 < 0$, also referred to as Brownian motion) or to DSs moving with a finite dynamically stabilized intrinsic velocity ($a_1 > 0$, $a_3 < 0$, also referred to as active Brownian motion [24, 25]).

A further interesting aspect can be mentioned: for the presented technique to work, the correlation time t_c of the fluctuation forces must be smaller than the distance Δt between two successive data points. By reducing Δt and carrying out the analysis for the same parameters, the correlation time can be estimated as the obtained results change and finally diverge if Δt gets in the range of t_c. From this condition, one finds that for the considered cases, t_c is somewhat smaller than a millisecond.

3.2. Extension to interaction phenomena

The described stochastic analysis technique being applicable to non-interacting individual filaments shall now be extended such that it can be used to determine the interaction between two filaments. To this end, the Langevin equations describing the dynamics of single DSs have to be appropriately extended. Accordingly, the following theoretically motivated assumptions on the nature of the interaction are made (see also section 5 below):

(i) only mutual interaction between the DSs is taken into account;

(ii) the interaction between the DSs occurs due to generalized central forces, i.e. the forces are directed along the connecting line of the filaments. This assumption can easily be proven using O(2)-symmetry arguments;

(iii) the dependence of the interaction law on the velocity of the filaments is weak and can be neglected.

Using these assumptions, equation (4) is extended in the following way (different filaments are represented by different indices i, j with $i \neq j$ and the sum convention is used):

$$\dot{\boldsymbol{v}}_i = h_v(v_i) \cdot \boldsymbol{e}_{\boldsymbol{v}_i} + F(|\boldsymbol{p}_i - \boldsymbol{p}_j|)\frac{\boldsymbol{p}_i - \boldsymbol{p}_j}{|\boldsymbol{p}_i - \boldsymbol{p}_j|} + R(v_i)\boldsymbol{\Gamma}_i(t), \tag{12}$$

where

$$\langle \Gamma_{i,\mu}(t) \rangle = 0, \qquad i = 1, \ldots, n, \quad \mu = x, y, \tag{13}$$

$$\langle \Gamma_{i,\mu}(t)\Gamma_{j,\nu}(t') \rangle = 2\delta_{ij}\delta_{\mu\nu}\delta(t - t'), \qquad i, j = 1, \ldots, n, \quad \mu, \nu = x, y. \tag{14}$$

To avoid the known problems from three- or many-body interaction, in the following, only the interaction between two DSs will be analysed. Although the form of the equation is motivated by theoretical models, one should try to find also an experimental confirmation of the additive nature of the interaction force. This can be achieved in the following way: with an appropriate choice of the system parameters, a multistable situation can be created in which both one and two DSs are stable solutions of the system. For the isolated DS, the dynamics can simply be analysed as described above. For the two-soliton state, intrinsic dynamics and interaction act

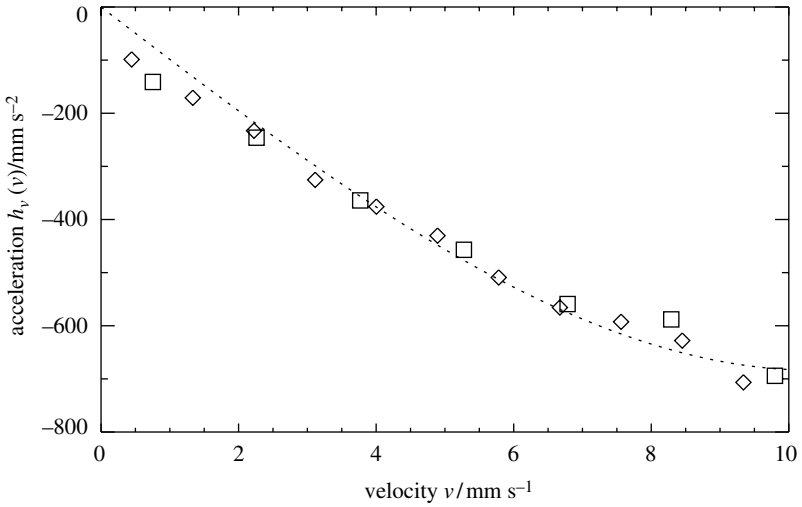

Figure 4. Deterministic part $h_v(v)$ of the dynamics for a multistable situation with one and two DSs. Squares: isolated DS, diamonds: two DSs. In addition, a cubic fit according to (11) with $a_1 = -98.95\,\mathrm{s}^{-1}$ and $a_3 = 0.307\,\mathrm{mm}^{-1}$ is shown. Parameters: $U_0 = 4600\,\mathrm{V}$, $\rho_{SC} = 3.5 \times 10^6\,\Omega\,\mathrm{cm}$, $R_0 = 4.4\,\mathrm{M}\Omega$, $p = 283\,\mathrm{hPa}$, $T = 100\,\mathrm{K}$, $d = 500\,\mu\mathrm{m}$, with $I = 235\,\mu\mathrm{A}$.

simultaneously, but one can make use of the fact that the interaction strength decays to zero if a critical distance between the DSs is exceeded, as a simple analysis of the statistical properties of the dynamics shows. Therefore, the dynamics in the discussed case should be the pure intrinsic dynamics of each DSs if they are far away from each other. This allows for the determination of the intrinsic dynamics also for two DSs. The result of the experimental investigation is shown in figure 4 proving that the intrinsic part of the dynamics is the same in both cases. This gives a further justification for the additive character of the interaction term.

In addition, it is possible to experimentally validate the assumptions made for the fluctuation terms. Here, two aspects play an important role. First, the fluctuations for one DS are assumed to be independent of the velocities of the other DSs, meaning that the fluctuations for the individual DSs are uncorrelated (see equation (14)). This crucial point can be checked in the following way: the motion of the DSs takes place on different timescales (cf e.g. figure 2). Whereas the motion on a short time scale of some milliseconds is dominated by the influence of the fluctuations, the dynamics on a longer time scale is due to both deterministic and stochastic contributions. Therefore, the simultaneous motion of two DSs on a short time scale was checked for a possible correlation with standard techniques, yielding a vanishing correlation coefficient. Secondly, the fluctuation strength is assumed to be independent of the number of DSs present in the system. This point is not as crucial as the first one as the stochastic data analysis techniques used in this paper are able to determine deterministic and stochastic parts of the dynamics individually. A difference would only result for the deterministic parts in the case of multiplicative noise if an interpretation according to Stratonovich was used, whereas in this paper an interpretation according to Itó is chosen. Nevertheless, the fluctuations for single and multiple DSs were analysed with the help of equation (9), yielding a good agreement in all considered cases.

Assuming the validity of equation (12), the question arises of how the interaction function can be determined from experimental data. Of course, the equation can be considered as a

Langevin equation in more than one random variable, allowing for an estimation following the scheme presented in equation (5). Similar to the analysis of single DSs, one faces the above-mentioned problem that the limited amount of experimentally available data points in the given case results in a poor resolution. However, the way of proceeding in the multistable situation opens up a possibility to determine $h_v(v)$ without having to determine $F(d)$. If h_v is known for a certain set of parameters, a new acceleration can be introduced as follows:

$$\dot{\boldsymbol{v}}_{i,n} := \dot{\boldsymbol{v}}_i - h_v(v_i)\boldsymbol{e}_{\boldsymbol{v}_i} = F(|\boldsymbol{p}_i - \boldsymbol{p}_j|)\frac{\boldsymbol{p}_i - \boldsymbol{p}_j}{|\boldsymbol{p}_i - \boldsymbol{p}_j|} + R(v_i)\boldsymbol{\Gamma}_i(t). \tag{15}$$

Now, the interaction law $F(d)$ with $d = |\boldsymbol{p}_i - \boldsymbol{p}_j|$ can be estimated using

$$F(d) = \left\langle \dot{\boldsymbol{v}}_{i,n} \cdot \frac{\boldsymbol{p}_i - \boldsymbol{p}_j}{|\boldsymbol{p}_i - \boldsymbol{p}_j|} \right\rangle \Bigg|_{|\boldsymbol{p}_i - \boldsymbol{p}_j| = d} \tag{16}$$

$$\approx \frac{1}{\Delta t}\left\langle (\boldsymbol{v}_i(t + \Delta t) - \boldsymbol{v}_i(t) - \Delta t h_v(v_i)\boldsymbol{e}_{v_i}) \cdot \frac{\boldsymbol{p}_i - \boldsymbol{p}_j}{|\boldsymbol{p}_i - \boldsymbol{p}_j|} \right\rangle \Bigg|_{|\boldsymbol{p}_i - \boldsymbol{p}_j| \approx d}. \tag{17}$$

A proof for this relation is given in appendix A2. With the presented method, the determination of $h_v(v)$ and $F(d)$ can take place separately using only one random variable for each estimation, thereby guaranteeing a maximal efficiency.

The only problem is that the critical radius r_C above which the interaction strength vanishes is not known exactly. To overcome this problem, one may in a first step assume a very large radius. With this radius, h_v is calculated using (10) neglecting the interaction. The following calculation of $F(d)$ using (17) reveals the existence of a new critical distance d_C, which is usually smaller than the first one. A better approximation for $F(d)$ is now iteratively computed in two steps:

(i) a new drift function $h_v(v)$ is determined according to (10) from data for which $d > d_C$ holds as, for these data, the interaction is assumed to be negligible and the amount of data that can be used for this step is usually greater than in the previous step;

(ii) a new interaction law $F(d)$ is calculated via equation (17) from the new $h_v(v)$ and data for which $d < d_C$ holds, yielding a new critical distance d_C for the next iteration.

Convergence of the iteration process is achieved once the critical distance d_C does not change significantly (usually, three to four steps are needed).

Before applying the discussed methods to experimental data, they were tested on data series numerically generated using appropriate Langevin equations, showing that the underlying equations are well reproduced by the stochastic data analysis.

4. Application to experimental data

In most cases, the fluctuations in the experimental system are much stronger than for the case depicted in figure 2. However, this fact has a positive influence on the efficiency of the presented technique as strong fluctuations are able to drive the system into highly transient states, which could not be analysed otherwise. A typical result of an interaction law $F(d)$ for experimentally observed current filaments, which was found under these conditions and which shows clearly the characteristic properties of the interaction, is depicted in figure 5 (black crosses). The alternating

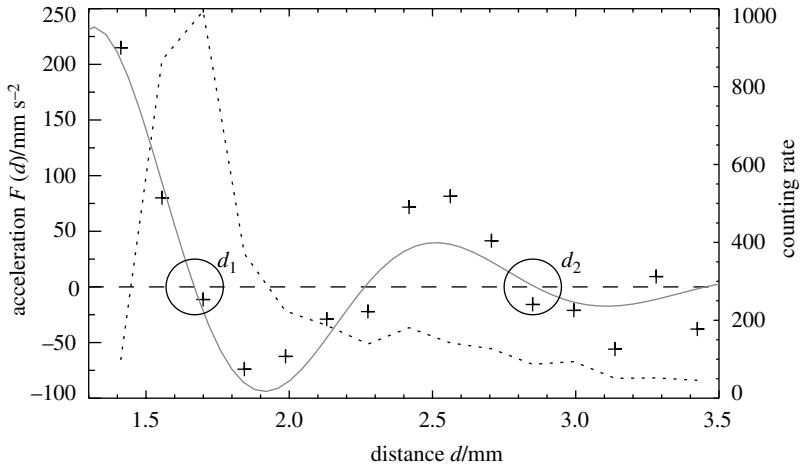

Figure 5. Acceleration $F(d)$ determined from 4050 experimental data points (crosses). The solid grey line is a fit according to (21), with $f_1 = 1386.6\,\mathrm{mm}^{3/2}\,\mathrm{s}^{-2}$, $f_2 = 1.2167\,\mathrm{mm}^{-1}$, $f_3 = 5.27957\,\mathrm{mm}^{-1}$ and $f_4 = 8.47037$. Parameters: $U_0 = 4600\,\mathrm{V}$, $\rho_{SC} = 3.5\,\mathrm{M\Omega\,cm}$, $R_0 = 4.4\,\mathrm{M\Omega}$, $p = 283\,\mathrm{hPa}$, $T = 100\,\mathrm{K}$, $d = 500\,\mu\mathrm{m}$, $t_{exp} = 0.02\,\mathrm{s}$ and $I = 235\,\mu\mathrm{A}$.

sign of the interaction law reflects spatial regions of attraction and repulsion, yielding two stable fixed points at $d_1 \approx 1.65\,\mathrm{mm}$ and $d_2 \approx 2.85\,\mathrm{mm}$. Note that for the actual parameter set the filament diameter was approximately $D = 0.8\,\mathrm{mm}$. Therefore, the investigated distance range in figure 5 clearly lies outside the core area of the filaments, guaranteeing for a theoretical modelling that the concept of weakly interacting filaments is a good approximation. Although the fluctuations were rather large in the presented example, one can see from the frequency polygon (dashed line), reflecting the probability of finding the DSs in a certain distance, that the probability for the DSs to take the distance d_1 is very high, yielding an independent confirmation of the measured result. In addition, the strong repulsive force for small distances explains the observation of typical minimal scattering distances.

Further analysis of recorded experimental trajectories shows that in most cases, the measured interaction law is qualitatively similar to the interaction law depicted in figure 5. In all cases, the direct observations and the found frequency polygons for the probability of finding are consistent with the interaction law resulting from the stochastic data analysis technique. Consequently, the measured interaction laws are also able to explain the transient formation of soliton molecules and clusters which may only exist if the proportion of intrinsic dynamics, interaction strength and fluctuation strength is appropriate.

5. Interpretation of the experimental findings

After being able to analyse the experimentally observable dynamics of the DSs, the question arises of how the findings can be understood. Up to this moment, no microscopic model for gas-discharge systems with the used planar geometry was investigated. However, a phenomenological three-component reaction–diffusion system on the basis of an electrical equivalent circuit was proposed for the investigated gas-discharge system [26, 27]. In this model, the central equations

are of the form

$$\begin{aligned}\dot{\mathrm{u}} &= d_u \Delta \mathrm{u} + \lambda \mathrm{u} - \mathrm{u}^3 - \kappa_3 \mathrm{v} - \kappa_4 \mathrm{w} + \kappa_1,\\ \tau \dot{\mathrm{v}} &= d_v \Delta \mathrm{v} + \mathrm{u} - \mathrm{v},\\ \theta \dot{\mathrm{w}} &= d_w \Delta \mathrm{w} + \mathrm{u} - \mathrm{w},\end{aligned} \tag{18}$$

where $\mathrm{u}(\boldsymbol{x}, t)$, $\mathrm{v}(\boldsymbol{x}, t)$ and $\mathrm{w}(\boldsymbol{x}, t)$ are elements of $C^2(\Omega \times \mathbb{R})$, Ω is a finite subset of $\mathbb{R}^2$, and d_u, d_v, d_w, λ, τ, θ, κ_1, κ_3 and κ_4 are positive constants. The activating component u is related to the production of charge carriers in the gas, the inhibiting component v is related to the voltage drop over the semiconductor and the inhibiting component w can be connected to surface charges on the gas–semiconductor interface [28].

The model system (18) exhibits particle-like solutions typically showing interaction phenomena such as scattering and formation of bound states, which is the reason why they are also referred to as DSs. To allow for an at least semi-quantitative comparison with the experimental findings, it is possible to reduce the partial differential equations (18) to ordinary differential equations by projecting them onto the critical modes of their linear part (see e.g. [11, 29] for mathematical details).

In the limit $d_v \to 0$ and $\theta \to 0$, one obtains the equation

$$\ddot{\boldsymbol{p}} = \dot{\boldsymbol{v}} = \kappa_3(\kappa_3\tau - 1)\boldsymbol{v} - \frac{Q}{\kappa_3}|\boldsymbol{v}|^2\boldsymbol{v}, \qquad Q = \frac{\langle \bar{\mathrm{u}}_{xx}^2 \rangle}{\langle \bar{\mathrm{u}}_x^2 \rangle} \tag{19}$$

for the acceleration of a single DS which is in good agreement with the experimental findings for single DSs (cf section 3.1 and also the extensive discussion of this fact in [18]). When reducing the partial differential equations to ordinary differential equations, it is also possible to take the mutual interaction of several DSs into account [11]. A further simplification of the equations for two interacting DSs i and j with $i \neq j$ by neglecting high-order terms [30] allows a reduction of the field equations (18) to ordinary differential equations describing the motion of the localized structures in the following form:

$$\dot{\boldsymbol{v}}_i = \kappa_3(\kappa_3\tau - 1)\boldsymbol{v}_i + \frac{Q}{\kappa_3}v_i^2\boldsymbol{v}_i + \kappa_3 F(|\boldsymbol{p}_i - \boldsymbol{p}_j|)\frac{\boldsymbol{p}_i - \boldsymbol{p}_j}{|\boldsymbol{p}_i - \boldsymbol{p}_j|}. \tag{20}$$

Due to the good agreement of the experimentally measured drift function of equation (11) and its theoretical equivalent (the first two terms on the right-hand side of equation (20)), one may be tempted to make an extension of the comparison between the model and the experimental findings to the interaction law $F(d)$. In the case of theoretically investigated DSs, the distance-dependent interaction law can be numerically calculated, showing for DSs capable of forming bound states a typical oscillatory behaviour (figure 6(a)), which can be very well fitted to the function

$$F(d) = -\frac{f_1}{\sqrt{d}}\mathrm{e}^{-f_2 d}\cos(f_3 d + f_4), \tag{21}$$

where f_i, $i = 1, \ldots, 4$, represent fit parameters (figure 6(b)). According to the model, the stable fixed points of the interaction function correspond to the relative maxima in the tails of the activator distribution of the DSs. In this way, bound states are formed when there is a 'constructive' overlapping of two or more DSs.

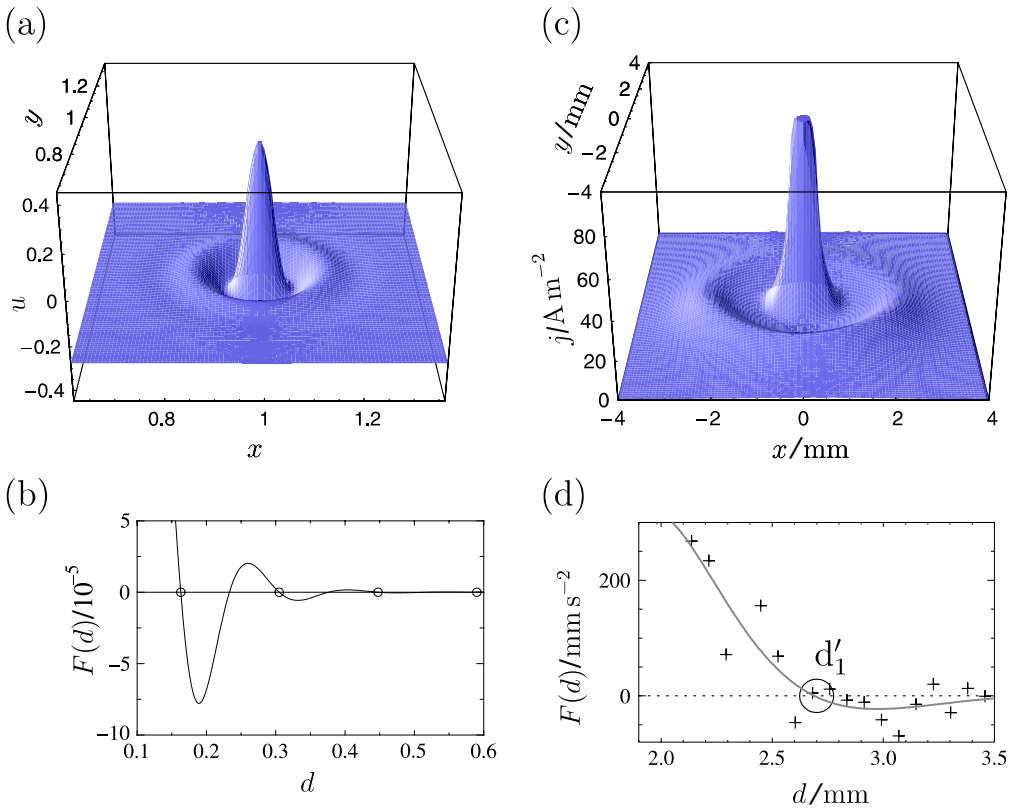

Figure 6. (a) Surface plot image of the activator distribution u of a DS with oscillatory tails, parameters: $d_{\mathbf{u}} = 1.1 \times 10^{-4}$, $d_{\mathbf{v}} = 0$, $d_{\mathbf{w}} = 9.64 \times 10^{-4}$, $\lambda = 1.01$, $\kappa_1 = -0.1$, $\kappa_3 = 0.3$, $\kappa_4 = 0.1$, $\tau = 3.32$ and $\theta = 0$. (b) The corresponding interaction function according to equation (20). (c) Current density distribution of an experimentally observed DS with oscillatory tails averaged over 1000 frames. Parameters: $U_0 = 3900\,\mathrm{V}$, $\rho_{SC} = 3.05\,\mathrm{M\Omega\,cm}$, $R_0 = 4.4\,\mathrm{M\Omega}$, $p = 279\,\mathrm{hPa}$, $T = 100\,\mathrm{K}$, $d = 500\,\mu\mathrm{m}$, $t_{exp} = 0.02\,\mathrm{s}$, with $I = 200\,\mu\mathrm{A}$. (d) Acceleration function $F(d)$ obtained from the experimental trajectories of two interacting filaments for the same parameters determined from 2000 data points (crosses). The solid grey line is a fit according to (21), with $f_1 = 63512.6\,\mathrm{mm^{3/2}\,s^{-2}}$, $f_2 = 2.03663\,\mathrm{mm^{-1}}$, $f_3 = 3.15296\,\mathrm{mm^{-1}}$ and $f_4 = 6.91006$.

It turns out that the theoretically obtained interaction function (21) is very well suited to fit the experimentally obtained interaction law shown in figure 5 (cf the thick grey curve). However, in the depicted case, it is not possible to find oscillatorily decaying tails in the average current density distribution. In spite of this, it is possible to experimentally find DSs exhibiting oscillatory tails for an appropriate choice of system parameters. Figure 6(c) shows an example in which the current density distribution of a DS was centred and averaged to exclude disturbances of the shape due to fluctuations and for which the oscillatory nature is clearly visible. In addition, it is also possible to determine an interaction law in this case which is depicted in figure 6(d). If one compares the stable fixed points of the interaction function with the maxima of the distribution, it is actually possible to find a good agreement with the theoretical predictions.

The question whether an oscillatory interaction law can always be connected to an oscillatory decay of the DSs as predicted by the phenomenological reaction–diffusion model is a matter of current investigations. However, numerical investigations of the theoretical model have shown that even very weakly pronounced oscillatory tails may have a significant influence on the interaction law, so that more sophisticated methods for the analysis of the distributions may have to be used.

6. Summary and outlook

Introducing a stochastic data analysis method, it is possible for the first time to measure the interaction law of DSs appearing in the form of current filaments in an experimental dc gas-discharge system. Making use of the fluctuations present in the experimental system, not only stationary but also transient states can be analysed. The interaction law gives a quantitative explanation for typical phenomena like scattering and the formation of bound states.

In addition, the current density distributions of the corresponding non-interacting DSs were analysed. In the case of oscillatorily decaying distributions, the positions of the stable fixed points of the interaction law agree with the positions of the maximum in the tail of the spatial distribution of the DS. This is in good agreement with model considerations and therefore a strong argument for the strength of the applied model. Furthermore, the quantitative results of the stochastic data analysis will allow for a comparison with microscopic models which are yet to be developed.

As the interaction of localized objects, possibly under the influence of noise, is of great interest for many different areas of modern science, e.g. reaction–diffusion systems, optics, hydrodynamic systems and even biological systems, the presented techniques may find many other fields of application. This holds especially for systems which possess translational invariance as, in these systems, the localized objects are susceptible to fluctuations due to the existence of neutral modes of translation. Possible direct fields of application are, e.g. the interaction of optical solitons [15] and DSs in driven fluids [16].

Acknowledgments

We gratfully acknowledge the support of this work by the Deutsche Forschungsgemeinschaft.

Appendix. Mathematics

The central concern of the appendix is to prove relation (10) for multiplicative noise and the projection technique (17) for the determination of the interaction function.

A1. Proof of equation (10)

To prove the validity of equation (10), one considers the Fokker–Planck equation belonging to (1), first in Cartesian coordinates:

$$\frac{\partial W(\boldsymbol{v},t)}{\partial t} = \left(-\frac{\partial}{\partial v_i}h_i(\boldsymbol{v},t) + \frac{\partial^2}{\partial v_i \partial v_j}R_{ij}(\boldsymbol{v},t)\right) W(\boldsymbol{v},t), \quad i,j = 1,2. \tag{A.1}$$

In the stationary case, one finds

$$\boldsymbol{h}(\boldsymbol{v}) = \lim_{\Delta t \to 0} \frac{1}{\Delta t} \int (\boldsymbol{V} - \boldsymbol{v}) P_{st}(\boldsymbol{V}, t + \Delta t | \boldsymbol{v}, t)\, \mathrm{d}^2 V, \tag{A.2}$$

where P_{st} is the conditional probability density for the Markovian process in the stationary case. For the function $\boldsymbol{h}(\boldsymbol{v})$, one chooses a representation in polar coordinates, first neglecting the isotropy condition in (4):

$$\boldsymbol{h}(\boldsymbol{v}) = h_v(\boldsymbol{v})\boldsymbol{e}_v(\varphi) + h_\varphi(\boldsymbol{v})\boldsymbol{e}_\varphi(\varphi). \tag{A.3}$$

Here, $h_v(\boldsymbol{v})$ and $h_\varphi(\boldsymbol{v})$ are the projections of $\boldsymbol{h}(\boldsymbol{v})$ onto the unit vectors in radial and azimuthal direction. Although $h_v(\boldsymbol{v})$ is defined using (A.2), $h_v(\boldsymbol{v})$ is indeed only a function of $\boldsymbol{v}$ (and does not explicitly depend on t), as for P the stationary solution P_{st} was used. Inserting the representation in polar coordinates into equation (A.2), one finds

$$\begin{aligned} h_v(\boldsymbol{v}) &= \frac{\boldsymbol{v}}{v} \cdot \boldsymbol{h}(\boldsymbol{v}) \\ &= \lim_{\Delta t \to 0} \frac{1}{\Delta t} \int \frac{\boldsymbol{v}}{v} \cdot (\boldsymbol{V} - \boldsymbol{v}) P_{st}(\boldsymbol{V}, t + \Delta t | \boldsymbol{v}, t)\, \mathrm{d}^2 V \\ &= \lim_{\Delta t \to 0} \frac{1}{\Delta t} \int \left(\frac{\boldsymbol{V} \cdot \boldsymbol{v}}{v} - v \right) P_{st}(\boldsymbol{V}, t + \Delta t | \boldsymbol{v}, t)\, \mathrm{d}^2 V. \end{aligned} \tag{A.4}$$

According to the above relation, let $\tilde{\boldsymbol{v}}(t)$ be the random variable for which $W(\boldsymbol{v}, t) = \langle \delta(\boldsymbol{v} - \tilde{\boldsymbol{v}}(t)) \rangle$. Using this definition in (A.4) yields

$$\begin{aligned} h_v(\boldsymbol{v}) &= \lim_{\Delta t \to 0} \left\langle \frac{\tilde{\boldsymbol{v}}(t + \Delta t) \cdot \boldsymbol{v}}{v} - v \right\rangle \Bigg|_{\tilde{\boldsymbol{v}} = \boldsymbol{v}} \\ &= \lim_{\Delta t \to 0} \left\langle \frac{\tilde{\boldsymbol{v}}(t + \Delta t) \cdot \tilde{\boldsymbol{v}}}{\tilde{v}} - \tilde{v} \right\rangle \Bigg|_{\tilde{\boldsymbol{v}} = \boldsymbol{v}}, \end{aligned} \tag{A.5}$$

independent of the nature of the fluctuations. In this way, the radial part of the deterministic function $\boldsymbol{h}(\boldsymbol{v})$ can be determined even without isotropy of the problem. In a similar way, the azimuthal part can be estimated:

$$\begin{aligned} h_\varphi(\boldsymbol{v}) &= \boldsymbol{e}_\varphi(\varphi) \cdot \boldsymbol{h}(\boldsymbol{v}) = \boldsymbol{e}_\varphi \left(\arctan\left(\frac{v_2}{v_1} \right) \right) \cdot \boldsymbol{h}(\boldsymbol{v}) \\ &= \lim_{\Delta t \to 0} \frac{1}{\Delta t} \int \left(\boldsymbol{e}_\varphi(\varphi) \cdot \boldsymbol{V} - \underbrace{\boldsymbol{e}_\varphi(\varphi) \cdot \boldsymbol{v}}_{=0} \right) P_{st}(\boldsymbol{V}, t + \Delta t | \boldsymbol{v}, t)\, \mathrm{d}^2 V \\ &= \lim_{\Delta t \to 0} \left\langle \tilde{\boldsymbol{v}}(t + \Delta t) \cdot \boldsymbol{e}_\varphi \left(\arctan\left(\frac{v_2}{v_1} \right) \right) \right\rangle \Bigg|_{\tilde{\boldsymbol{v}} = \boldsymbol{v}}. \end{aligned} \tag{A.6}$$

If the azimuthal part vanishes, then $h_v(\boldsymbol{v}) = h_v(v)$ and $h_\varphi(\boldsymbol{v}) = 0$ hold. Then, the left-hand side of (A.5) is independent of φ, and one arrives at

$$h_v(v) = \lim_{\Delta t \to 0} \left\langle \frac{\tilde{\boldsymbol{v}}(t+\Delta t)\cdot\tilde{\boldsymbol{v}}}{\tilde{v}} - \tilde{v} \right\rangle \Bigg|_{|\tilde{\boldsymbol{v}}|=v}. \tag{A.7}$$

This corresponds to equation (10).

A2. Proof of equation (17)

The central Langevin equation for the determination of the generalized interaction force between two DSs is equation (12). By subtracting the drift term $\boldsymbol{h}(\boldsymbol{v})$ on both sides of the equation, one arrives at equation (15) as the basis for the application of the analysis technique. The equation is of the form

$$\dot{\boldsymbol{v}}_i - h_v(v_i)\boldsymbol{e}_{v_i} = f(\boldsymbol{d}_{ij}(t))\frac{\boldsymbol{d}_{ij}}{d_{ij}} + R(v_i)\boldsymbol{\Gamma}_i(t) \tag{A.8}$$

with $R > 0$, $\boldsymbol{v}_i = (v_{i,x}, v_{i,y})^{\mathrm{T}}$, $\boldsymbol{d}_{ij} = (\boldsymbol{p}_i - \boldsymbol{p}_j)$, $\boldsymbol{p}_i = (p_{i,x}, p_{i,y})^{\mathrm{T}}$ and $i, j = 1, 2$, $i \neq j$. For the fluctuation term $\boldsymbol{\Gamma}_i = (\Gamma_{i,x}, \Gamma_{i,y})^{\mathrm{T}}$, one assumes (13) and (14) to hold. The random variables are therefore $\boldsymbol{v}_i$, $\dot{\boldsymbol{v}}_i$, $\boldsymbol{d}_{ij}$ and $\boldsymbol{\Gamma}_i$.

If one considers equation (A.8) for fixed $\boldsymbol{v}_i$ and for fixed $\boldsymbol{d}_{ij}$, i.e. $\boldsymbol{v}_i(t) = \boldsymbol{v}_i^*$ and $\boldsymbol{d}_{ij}(t) = \boldsymbol{d}_{ij}^*$, one arrives at

$$\dot{\boldsymbol{v}}_i|_{\boldsymbol{v}_i=\boldsymbol{v}_i^*} - h_v(v_i^*)\boldsymbol{e}_{v_i^*} = f(\boldsymbol{d}_{ij}^*)\frac{\boldsymbol{d}_{ij}^*}{d_{ij}^*} + R(v_i^*)\boldsymbol{\Gamma}_i(t). \tag{A.9}$$

The random variables are now only $\dot{\boldsymbol{v}}_i$ and $\boldsymbol{\Gamma}_i$. One exploits the Itó calculus and takes the ensemble average $\langle \ldots \rangle$ on both sides of the equation, obtaining

$$\langle \dot{\boldsymbol{v}}_i \rangle|_{\boldsymbol{v}_i=\boldsymbol{v}_i^*} - h_v(v_i^*)\boldsymbol{e}_{v_i^*} = f(\boldsymbol{d}_{ij}^*)\frac{\boldsymbol{d}_{ij}^*}{d_{ij}^*} + R(v_i^*)\underbrace{\langle \boldsymbol{\Gamma}_i(t) \rangle}_{0}. \tag{A.10}$$

Both sides of the equation are multiplied with $\boldsymbol{d}_{ij}^*/d_{ij}^*$, yielding

$$f(\boldsymbol{d}_{ij}^*) = \frac{\boldsymbol{d}_{ij}^*}{d_{ij}^*} \cdot [\langle \dot{\boldsymbol{v}}_i \rangle|_{\boldsymbol{v}_i=\boldsymbol{v}_i^*} - h_v(v_i^*)\boldsymbol{e}_{v_i^*}]. \tag{A.11}$$

As this relation holds for all $\boldsymbol{v}_i^*$, the restriction $\boldsymbol{v}_i = \boldsymbol{v}_i^*$ can be dropped:

$$f(\boldsymbol{d}_{ij}^*) = \frac{\boldsymbol{d}_{ij}^*}{d_{ij}^*} \cdot [\langle \dot{\boldsymbol{v}}_i \rangle - h_v(v_i)\boldsymbol{e}_{v_i}]. \tag{A.12}$$

If one assumes that $f(\boldsymbol{d}_{ij}) = F(d_{ij})$, the left-hand side of equation (A.12) yields the same value for all $d_{ij}^* = d^*$. This results in

$$F(d^*) = \frac{\boldsymbol{d}_{ij}^*}{d^*} \cdot [\langle \dot{\boldsymbol{v}}_i \rangle - h_v(v_i)\boldsymbol{e}_{v_i}]|_{d_{ij}^*=d^*}. \tag{A.13}$$

In the next step, one defines a new variable $\boldsymbol{a}_i(\Delta t) = \boldsymbol{v}_i(t+\Delta t) - \boldsymbol{v}_i(t) - \Delta t h_v(v_i)\boldsymbol{e}_{v_i}$:

$$F(d^*) = \frac{\boldsymbol{d}_{ij}^*}{d^*} \cdot \left[\left\langle \lim_{\Delta t\to 0} \frac{\boldsymbol{a}_i(\Delta t)}{\Delta t}\right\rangle\right]\Bigg|_{d_{ij}^*=d^*}. \tag{A.14}$$

For arbitrary quantities A, the ensemble average is defined as

$$\langle \boldsymbol{A}\rangle = \lim_{N\to\infty} \frac{1}{N}\sum_{l=1}^{N} \boldsymbol{A}^l, \tag{A.15}$$

where the A^l are realizations of A. It is now reasonable to choose $\boldsymbol{A} = \boldsymbol{a}_i \cdot \boldsymbol{d}_{ij}^*/[d^*\,\Delta t]$, which results in

$$F(d^*) = \frac{1}{d^*} \lim_{N\to\infty} \lim_{\Delta t\to 0} \frac{1}{N\Delta t} \sum_{l=1}^{N} \boldsymbol{a}_i^l(\Delta t)\cdot \boldsymbol{d}_{ij}^*\Bigg|_{d_{ij}^*=d^*}. \tag{A.16}$$

If one assumes that the times for the ensemble average and for the time derivative can be exchanged, equation (A.16) can be transformed to

$$\begin{aligned} F(d^*) &= \frac{1}{d^*} \lim_{\Delta t\to 0} \lim_{N\to\infty} \frac{1}{N\Delta t} \sum_{l=1}^{N} \boldsymbol{a}_i^l(\Delta t)\cdot \boldsymbol{d}_{ij}^*\Bigg|_{d_{ij}^*=d^*} \\ &= \frac{1}{d^*} \lim_{\Delta t\to 0} \frac{1}{\Delta t} \langle \mathbf{a}_i^l(\Delta t)\cdot \boldsymbol{d}_{ij}^*\rangle\big|_{d_{ij}^*=d^*} \\ &= \lim_{\Delta t\to 0} \frac{1}{\Delta t} \left\langle \boldsymbol{a}_i^l(\Delta t)\cdot \frac{\boldsymbol{d}_{ij}^*}{d_{ij}^*}\right\rangle\Bigg|_{d_{ij}^*=d^*}. \end{aligned} \tag{A.17}$$

Therefore, the interaction can be approximately determined from experimentally recorded data series according to

$$F(d^*) \approx \frac{1}{\Delta t}\left\langle \boldsymbol{a}_i^l(\Delta t)\cdot \frac{\boldsymbol{d}_{ij}^*}{d_{ij}^*}\right\rangle\Bigg|_{d_{ij}^*=d^*}. \tag{A.18}$$

Inserting the definitions of $\boldsymbol{d}_{ij}$ and $\boldsymbol{a}_i$ given above, one obtains equation (17). To avoid the problem of the exchange of the limits in (A.17), one can already do the approximation performed in (A.18) in equation (A.9):

$$\boldsymbol{v}_i(t+\Delta t)|_{\boldsymbol{v}_i(t)=\boldsymbol{v}_i^*} - \boldsymbol{v}_i^* - \Delta t h_v(v_i^*)\boldsymbol{e}_{v_i^*} \approx \Delta t f(\boldsymbol{d}_{ij}^*)\frac{\boldsymbol{d}_{ij}^*}{d_{ij}^*} + \sqrt{\Delta t} R(v_i^*)\boldsymbol{\Gamma}_i(t). \tag{A.19}$$

The remaining consideration are then done analogously. The disadvantage of this way of proceeding is that by this simplification, the mathematical rigour of the proof is lost in an early step. In addition, the proof can also be done using an interpretation of the fluctuations according to Stratonovich by exchanging $\boldsymbol{h}(\boldsymbol{v})$ with $\hat{\boldsymbol{h}}(\boldsymbol{v})$ (cf equation (7)).

References

[1] Christov C I and Velarde M G 1995 *Physica* D **86** 323
[2] Bode M and Purwins H-G 1995 *Physica* D **86** 53
[3] Hodgkin A L and Huxley A F 1952 *J. Physiol.* **117** 500
[4] Ouyang Q, Castets V, Boissonade J, Roux J C, De Kepper P and Swinney H L 1991 *J. Chem. Phys.* **95** 351
[5] Rotermund H H, Jakubith S, von Oertzen A and Ertl G 1991 *Phys. Rev. Lett.* **66** 3083
[6] Lee K-J, McCormick W D, Pearson J E and Swinney H L 1994 *Nature* **369** 215
[7] Arecchi F T, Boccaletti S and Ramazza P 1999 *Phys. Rep.* **328** 1
[8] Ackemann T and Lange W 2001 *Appl. Phys.* B **72** 21
[9] Crawford C and Riecke H 1999 *Physica* D **129** 83
[10] Coulett P, Riera C and Tresser C 2000 *Phys. Rev. Lett.* **84** 3069
[11] Bode M, Liehr A W, Schenk C P and Purwins H-G 2002 *Physica* D **161** 45
[12] Umbanhowar P B, Melo F and Swinney H L 1996 *Nature* **382** 793
[13] Schäpers B, Feldmann M, Ackemann T and Lange W 2000 *Phys. Rev. Lett.* **85** 748
[14] Astrov Yu A and Logvin Yu A 1997 *Phys. Rev. Lett.* **79** 2983
[15] Falkovich G E, Stepanov M G and Turitsyn S K 2001 *Phys. Rev.* E **64** 067602
[16] Fineberg J and Lioubashevski O 1998 *Physica* A **249** 10
[17] Siegert S, Friedrich R and Peinke J 1998 *Phys. Lett.* A **243** 275
[18] Bödeker H U, Röttger M C, Liehr A W, Frank T D, Friedrich R and Purwins H-G 2003 *Phys. Rev.* E **67** 056220
[19] Liehr A W, Bödeker H U, Röttger M C, Frank T D, Friedrich R and Purwins H-G 2003 *New J. Phys.* **5** 89
[20] Ammelt E, Astrov Yu A and Purwins H G 1998 *Phys. Rev.* E **58** 7109
[21] Marchenko V M, Matern S, Astrov Yu A, Portsel L M and Purwins H-G 2002 *Proc. SPIE* **4669** 1
[22] Risken H 1996 *The Fokker-Planck-Equation. Methods of Solution and Applications* (Berlin: Springer)
[23] Hänggi P 1978 *Helv. Phys. Acta* **51** 183
[24] Erdmann U, Ebeling W, Schimansky-Geier L and Schweitzer F 2000 *Eur. Phys. J.* B **15** 105
[25] Schweitzer F 2003 *Brownian Agents and Active Particles. Collective Dynamics in the Natural and Social Sciences* (*Springer Ser. Symp.* vol 16) (Berlin: Springer)
[26] Schenk C P, Or-Guil M, Bode M and Purwins H-G 1997 *Phys. Rev. Lett.* **78** 3781
[27] Liehr A W, Moskalenko A W, Astrov Yu A, Bode M and Purwins H-G 2004 *Eur. Phys. J.* B **37** 199
[28] Gurevich E L, Liehr A W, Amiranashvili Sh and Purwins H-G 2004 *Phys. Rev.* E **69** 036211
[29] Bode M 1997 *Physica* D **106** 270
[30] Moskalenko A S 2002 *Master's Thesis* Institut für Angewandte Physik, Westfälische Wilhelms-Universität Münster